

Cancer Therapy

How to cite: *Angew. Chem. Int. Ed.* **2021**, *60*, 17570–17578

International Edition: doi.org/10.1002/anie.202103721

German Edition: doi.org/10.1002/ange.202103721

Supramolecular Polymerization-Induced Nanoassemblies for Self-Augmented Cascade Chemotherapy and Chemodynamic Therapy of Tumor

Kuikun Yang⁺, Guocan Yu⁺, Zhiqing Yang, Ludan Yue, Xiangjun Zhang, Chen Sun, Jianwen Wei, Lang Rao, Xiaoyuan Chen,^{*} and Ruibing Wang^{*}

Abstract: The clinical application of chemodynamic therapy is impeded by the insufficient intracellular H_2O_2 level in tumor tissues. Herein, we developed a supramolecular nanoparticle via a simple one-step supramolecular polymerization-induced self-assembly process using platinum (IV) complex-modified β -cyclodextrin-ferrocene conjugates as supramolecular monomers. The supramolecular nanoparticles could dissociate rapidly upon exposure to endogenous H_2O_2 in the tumor and release hydroxyl radicals as well as platinum (IV) prodrugs *in situ*, which is reduced into cisplatin to significantly promote the generation of H_2O_2 in the tumor tissue. Thus, the supramolecular nanomedicine overcomes the limitation of conventional chemodynamic therapy via the self-augmented cascade radical generation and drug release. In addition, dissociated supramolecular nanoparticles could be readily excreted from the body via renal clearance to effectively avoid systemic toxicity and ensure long term biocompatibility of the nanomedicine. This work may provide new insights on the design and development of novel supramolecular nanoassemblies for cascade chemo/chemodynamic therapy.

Introduction

Chemodynamic therapy (CDT) has emerged as an efficient strategy to combat tumors by converting endogenous H_2O_2 into highly toxic reactive oxygen species (ROS) via Fenton chemistry to destroy cancer cells.^[1] As the ROS generation shows no dependence on the external excitation or

local oxygen levels, CDT could be an ideal strategy to inhibit the growth of deep-seated, hypoxic tumors that are not readily accessible by the widely applied photodynamic cancer therapy. However, the therapeutic outcomes of CDT are highly dependent on the amount of endogenous H_2O_2 , which significantly comprises the antitumor effects, thereby promoting scientists to incorporate additional therapeutic modalities into conventional CDT strategies to improve their anticancer efficacy.^[2]

Platinum drugs are one of the most common chemotherapeutics and make up 50% of all the clinical anticancer drugs.^[3] Apart from the chemotherapeutic effect, platinum drugs can specifically activate nicotinamide adenine dinucleotide phosphate oxidase (NOX) in cancer cells to generate $O_2^{\cdot-}$ from O_2 , which is further dismutated by superoxide dismutase (SOD) to produce H_2O_2 .^[4] Therefore cisplatin-mediated chemotherapy could be an ideal supplement of CDT via continuous production of H_2O_2 as the power source for Fenton-like reactions. Although a variety of platforms have been developed to combine CDT with cisplatin-based chemotherapy for cancer treatment, efficient co-delivery of cisplatin and CDT agents into tumors always relies on drug delivery systems that inevitably suffer from complicated synthetic routes, insufficient drug loading, uncontrollable drug ratio, premature leakage and slow release of payloads as well as potential long term toxicity owing to the slow clearance of the delivery vehicles.^[5] For instance, Yang and co-workers developed a semiconducting perylene diimide

[*] Dr. K. Yang,^[†] Z. Yang, L. Yue, Dr. X. Zhang, C. Sun, J. Wei, Prof. R. Wang
State Key Laboratory of Quality Research in Chinese Medicine, Institute of Chinese Medical Science, University of Macau Avenida da Universidade, Taipa, Macau (China)
and
MoE Frontiers Science Center for Precision Oncology, University of Macau
Avenida da Universidade, Taipa, Macau (China)
E-mail: rwang@um.edu.mo
Dr. G. Yu^[†]
Key Lab of Organic Optoelectronics & Molecular Engineering, Department of Chemistry, Tsinghua University
Beijing (China)
Dr. L. Rao
Institute of Biomedical Health Technology and Engineering, Shenzhen Bay Laboratory
Shenzhen (China)

Prof. X. Chen
Departments of Diagnostic Radiology, Surgery, Chemical and Biomolecular Engineering and Biomedical Engineering, Yong Loo Lin School of Medicine and Faculty of Engineering, National University of Singapore
Singapore (Singapore)
and
Clinical Imaging Research Centre, Centre for Translational Medicine, Yong Loo Lin School of Medicine, National University of Singapore
Singapore (Singapore)
and
Nanomedicine Translational Research Program, NUS Center for Nanomedicine, Yong Loo Lin School of Medicine, National University of Singapore
Singapore (Singapore)
E-mail: chen.shawn@nus.edu.sg

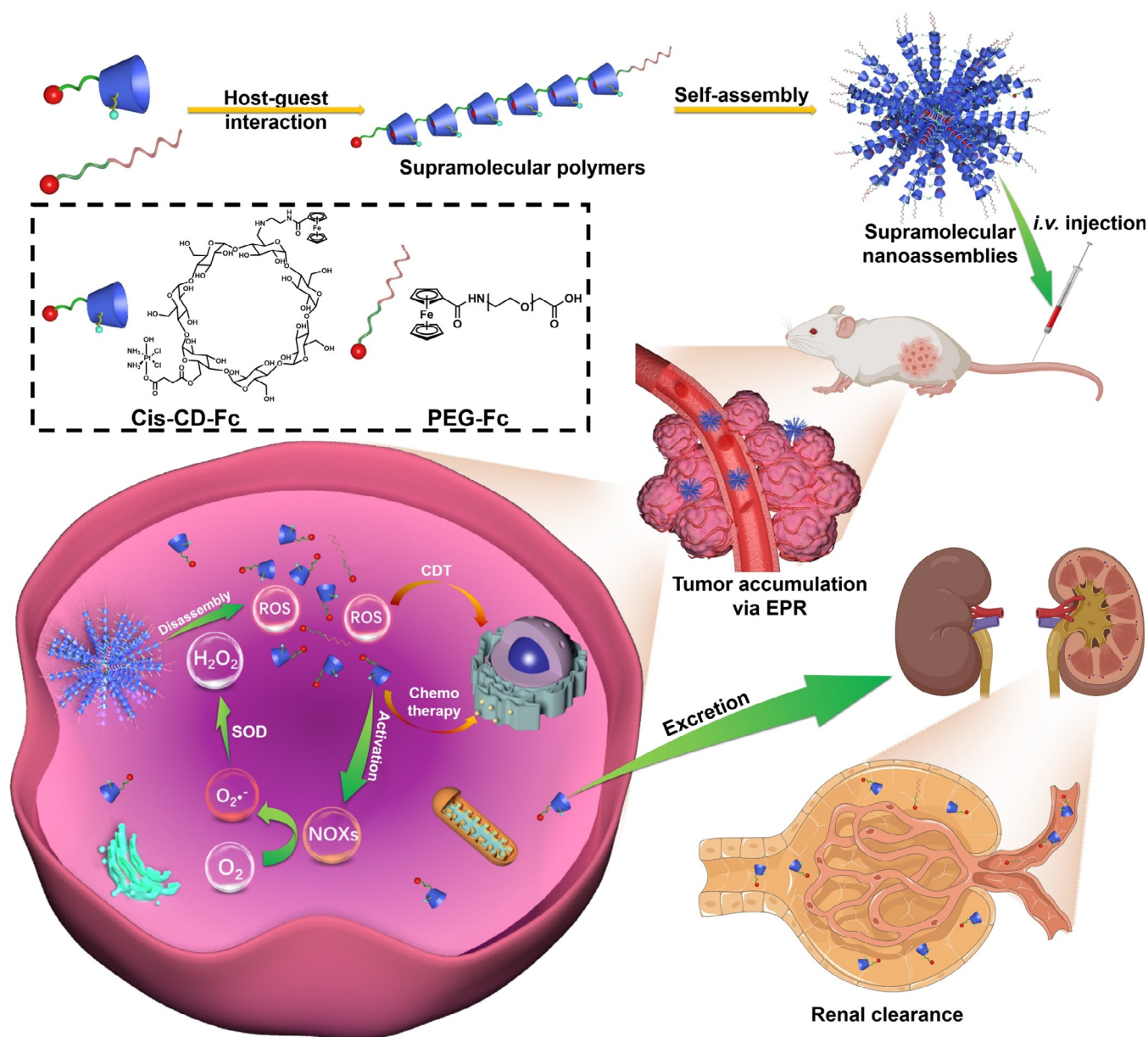
[†] These authors contributed equally to this work.

Supporting information and the ORCID identification number(s) for the author(s) of this article can be found under:
https://doi.org/10.1002/anie.202103721.

(PDI)-based theranostic NP for synergistic chemodynamic therapy and chemotherapy.^[6] The nanoparticle was assembled from PDI-based cisplatin prodrug and ferric ions, with polyethylene glycol (PEG) linked to the other amide group of PDI to enhance water solubility and biocompatibility of the nanopatform. Although the nanoparticles exhibited effective tumor growth inhibition, the sophisticated design and synthesis of the asymmetric PDI prodrug significantly restricts the clinical translation of the nanomedicine. In another work by Ren and co-workers, an organic theranostic nanomedicine (PTCG NPs) was constructed on the basis of the coordination interactions between iron ions (Fe^{3+}) and polyphenol-based polymers and prodrugs.^[5c] The high loading content of 5-hydroxydopamine modified platinum (IV) prodrug and iron ions enables combinational chemo/chemodynamic therapy

via cascade reactions. However, it remains challenging to precisely adjust the ratio between platinum (IV) prodrug and iron ions for optimized synergistic therapy. Therefore, it is extremely meaningful but challenging to construct a simple, safe and efficient delivery platform with tunable ratio and release behaviors of platinum drugs and CDT catalysts for synergistic chemo/chemodynamic cancer therapy.

Recently, supramolecular polymers (SPs) have been utilized to construct nanosized delivery platforms for tumor specific bioimaging and chemotherapy.^[7] Different from traditional polymers, the repeating units in the SPs are connected via directional and reversible noncovalent interactions, making it possible to introduce stimuli-responsiveness to the resultant supramolecular polymeric nanomaterials for various biomedical applications.^[8] In addition, imaging or



Scheme 1. H_2O_2 -responsive dissociation of PCSNs for self-augmented chemo/chemodynamic cancer therapy with rapid renal clearance of dissociated nanocarriers to minimize systemic toxicity and side effects.

therapeutic agents could be polymerized directly as the monomers to construct SPs owing to their strong binding affinity towards various hosts, resulting in nanomedicines with relatively high drug loading content and well-controlled composition. Although several SPs have been developed on the basis of supramolecular interactions between macrocyclic hosts and imaging/chemotherapeutic agents, rare examples were reported to construct SPs by using Fenton reagents as the guests for cancer treatment.^[9] As a typical CDT catalyst, ferrocene (Fc) shows strong affinity towards macrocyclic hosts such as β -cyclodextrin (CD), suggesting the potential of β -cyclodextrin-ferrocene conjugates (CD-Fc) in the construction of SPs for chemodynamic tumor therapy.^[10] Moreover, platinum (IV) prodrugs could be integrated into the CD-Fc-based SPs to further improve the therapeutic efficiency and reduce the side effects of the supramolecular nanomedicine.

Here we designed and synthesized a platinum (IV) complex-modified CD-Fc conjugates (Cis-CD-Fc) as supramolecular monomers, where the hydrophobic Fc guest and platinum (IV) prodrug are covalently conjugated with the hydrophilic CD host. The resultant supramolecular monomers could form linear SPs with Fc residing in the cavity of CD, which subsequently self-assemble into nanoparticles driven by the colloidal amphiphilicity of the SPs (Scheme 1). The design and construction of Cis-CD-Fc-based SPs for tumor specific delivery of chemotherapy and CDT was based on the following considerations: 1) The supramolecular nanoassemblies were obtained via a simple one-step supramolecular polymerization-induced self-assembly process, which significantly simplifies the fabrication and facilitates the clinical translation of the nanomedicine. 2) The drug loading capacity of the supramolecular nanoparticles (SNs) could be significantly improved as the payloads are part of the matrices, and the relative ratio of platinum (IV) complex and Fc could be precisely controlled by adjusting the monomer composition for supramolecular polymerization. 3) Hydrophobic Fc could be oxidized into hydrophilic ferrocenium by endogenous H_2O_2 via a Fenton-like reaction and release highly toxic hydroxyl radicals as a byproduct.^[11] In addition, ferrocenium exhibits significantly reduced binding affinity towards CD in comparison with Fc.^[12] Therefore, the Cis-CD-Fc-based supramolecular nanoassemblies could undergo rapid dissociation in the presence of endogenous H_2O_2 overproduced in tumors and release large amounts of hydroxyl radicals to induce tumor cell death for efficient CDT of tumors with abundant H_2O_2 (e.g. melanoma, lung, ovarian, colon and breast cancers).^[13] 4) The tumor-specific dissociation of SNs would be accompanied by the release of platinum (IV) prodrugs which is subsequently reduced to cisplatin for both chemotherapeutic effect and promoted generation of H_2O_2 at the tumor site, thus further accelerating the dissociation of the supramolecular nanocarriers. The cascade generation of ROS and burst release of platinum (IV) complex could enhance the antitumor efficacy through synergistic chemo/chemodynamic therapy. 5) The tumor-specific release of platinum (IV) prodrugs ensures minimized *in vivo* toxicity of the supramolecular nanomedicine to the normal tissues. In addition, the rapid dissociation of SNs and renal clearance of the resultant residues from the body could

minimize any side effect involving long term retention of the drug carriers.

Results and Discussion

Synthesis and Characterization of Supramolecular Polymers

The host-guest interaction between CD and Fc was first investigated by spectroscopic titration before synthesis of supramolecular monomers. With the gradual increase of CD concentration in an aqueous solution of CD and Fc, the characteristic absorption of Fc increased accordingly owing to the enhanced solubility of Fc in the solution (Figure S1). The stoichiometry was calculated to be 1:1 for the host-guest complex and the association constant between CD and Fc was calculated to be $1.90 \times 10^3 M^{-1}$ by using a nonlinear curve-fitting method (Figure S2 and S3), which is consistent with previously reported values.^[14] The formation of an inclusion complex between CD and Fc was also confirmed by 1H NMR, where the characteristic peak of Fc at 4.16 ppm disappeared with the addition of excess CD (Figure S4). Nuclear Overhauser effect correlations were found between the protons on Fc and CD in the 2D NOSEY spectrum, suggesting the deep penetration of the two parallel cyclopentadiene rings of Fc into the cavity of CD via hydrophobic interactions (Figure S5).

The supramolecular monomers of CD-Fc were synthesized via the amidation reaction of ferrocenecarboxylic acid N-succinimidyl ester with mono-(6-ethanediamine-6-deoxy)- β -cyclodextrin (Figure S6 and S7). The resultant CD-Fc was further conjugated with cisplatin (IV) prodrugs via the esterification reaction (Figure S8–S10). The solubility of Fc increased slightly from 0.15 to 53.3 $\mu g mL^{-1}$ in the presence of excess CD in the solution, and dramatically increased to 653.0 and 592.4 $\mu g mL^{-1}$ upon formation of supramolecular monomers of CD-Fc and Cis-CD-Fc, respectively (Figure S11). Therefore the improved solubility of Fc in supramolecular monomers could be ascribed to both the supramolecular interactions and the covalent conjugation of Fc and CD, indicating the potential of the supramolecular monomers to form SPs in an aqueous solution.

2D diffusion-ordered NMR spectroscopy (DOSY) was applied to investigate the supramolecular polymerization of CD-Fc and Cis-CD-Fc in aqueous solutions (Figure S12). The measured weighted average diffusion coefficients of both CD-Fc and Cis-CD-Fc decreased significantly when the concentration of the corresponding monomers increased from 0.1 to 4.0 mM. In contrast, the mixture of CD and Fc showed little decrease in diffusion coefficients with an increased concentration, suggesting the concentration-dependent supramolecular polymerization of CD-Fc and Cis-CD-Fc monomers.^[15] The molecular weight of Cis-CD-Fc increased from 2.0 to 27.2 kDa as the concentration of supramolecular monomers increased from 0.1 to 4.0 mM, further confirming the formation of SPs at high concentration of Cis-CD-Fc monomers (Figure S13).

Supramolecular Polymerization-Induced Self-Assembly

Poly (ethylene glycol) (MW: 2000) terminated by Fc (PEG-Fc) was designed and synthesized to initiate the supramolecular polymerization-induced self-assembly of CD-Fc or Cis-CD-Fc monomers (Figure S14 and S15). Here PEG-Fc was introduced to 1) control the length of SPs by adjusting the ratio of PEG-Fc to the supramolecular monomers; 2) confer hydrophilicity to the system to induce self-assembly of the resultant supramolecular diblock copolymers and 3) create steric hindrance for plasma proteins to improve the in vivo stability and prolong the blood circulation of the resultant supramolecular nanoassemblies.^[16] Transmission electron microscope (TEM) images illustrated the formation of well-defined nanoparticles from PEG-Fc terminated CD-Fc or Cis-CD-Fc SPs via the one-pot supramolecular polymerization-induced self-assembly process without any further purification (Figure 1A and S16). Apart from SNs, the morphology of the supramolecular assemblies could be well turned by adjusting the length of the supramolecular segment. Using Cis-CD-Fc as a prototype system, we systematically varied the concentration and relative ratio between PEG-Fc and supramolecular monomers to obtain SPs with different lengths and the morphology of the corresponding supramolecular assemblies was summarized in a phase diagram to guide the reproducible preparation of morphologically pure

nanoassemblies (Figure 1B). For instance, irregular aggregates were observed at a low concentration of both PEG-Fc and Cis-CD-Fc, probably owing to the failure of supramolecular polymerization of the scarce monomers (Figure 1C). Microfibers were found with an increased concentration of Cis-CD-Fc monomers, indicating the unlimited growth of SPs in the absence of sufficient PEG-Fc to terminate the polymerization (Figure 1D). With an increased concentration of both PEG-Fc and Cis-CD-Fc, well-defined SNs were obtained at an appropriate ratio of PEG-Fc and Cis-CD-Fc (Figure 1E). However, further increasing the amount of Cis-CD-Fc resulted in a mixture of SNs and microfibers owing to the lack of hydrophilic PEG-Fc to induce the self-assembly (Figure 1F). On the contrary, ultrasmall supramolecular dots (≈ 5 nm) were observed when abundant PEG-Fc was added into the Cis-CD-Fc solution (Figure 1G). In the presence of concentrated PEG-Fc, short supramolecular oligomers were formed instead of SPs. As a result, ultrasmall supramolecular dots were obtained owing to the deficient hydrophobicity required for the assembly of SNs. This was confirmed by the decreased molecular weight of SPs from 18.7 to 5.2 kDa when the relative ratio of PEG-Fc to Cis-CD-Fc increased from 1:20 to 1:2 (Figure S17). The SNs assembled from Cis-CD-Fc SPs (PCSNs) showed a positive zeta potential of 21.1 ± 7.2 mV and a hydrodynamic diameter of 91.6 ± 14.3 nm, which is beneficial for their accumulation in tumor tissues via the enhanced permeability and retention (EPR) effect as compared with other supramolecular assemblies (Figure 1H,I and S18).^[17] Moreover, the high-angle annular dark-field scanning TEM (HAADF-STEM)-based elemental mapping indicated the uniform distribution of Fe, Pt and Cl elements in the PCSNs, further confirming the supramolecular polymerization-induced self-assembly of Cis-CD-Fc monomers (Figure 1J). Therefore, PCSNs were employed for the following antitumor studies.

The loading content and relative ratio of the loaded platinum (IV) complex and Fc could be accurately controlled in the SNs by simply adjusting the composition of the supramolecular monomers. Here a series of SPs were prepared with multiple fixed-ratio combinations of CD-Fc and Cis-CD-Fc as supramolecular monomers to construct SNs (Figure S19). The loading content of cisplatin (IV) prodrugs increased from 2.2% to 12.2% while the loading content of Fc slightly decreased from 14.1% to 9.2% with an increasing content of Cis-CD-Fc from 20% to 100% in the SPs (Figure S20). In order to find the optimal ratio between CD-Fc and Cis-CD-Fc for further in vitro and in vivo studies, the synergistic chemo/chemodynamic effect of various SNs on mouse 4T1 breast cancer cells was investigated using the 3-(4,5-dimethylthiazol-2-yl)-2,5-diphenyltetrazolium bromide (MTT) assay (Figure S21).^[18] The combination index (CI) of each formulation was calculated by using a Chou-Talalay method to identify the most efficacious combination of CD-Fc and Cis-CD-Fc for antitumor studies (Figure S22).^[19] A strong synergistic effect was observed for all the SNs, and the CI value reached the lowest (CI=0.25) when the supramolecular assemblies were composed of pure Cis-CD-Fc, indicating the strongest synergistic chemo/chemodynamic effect of PCSNs in comparison with other formulations of

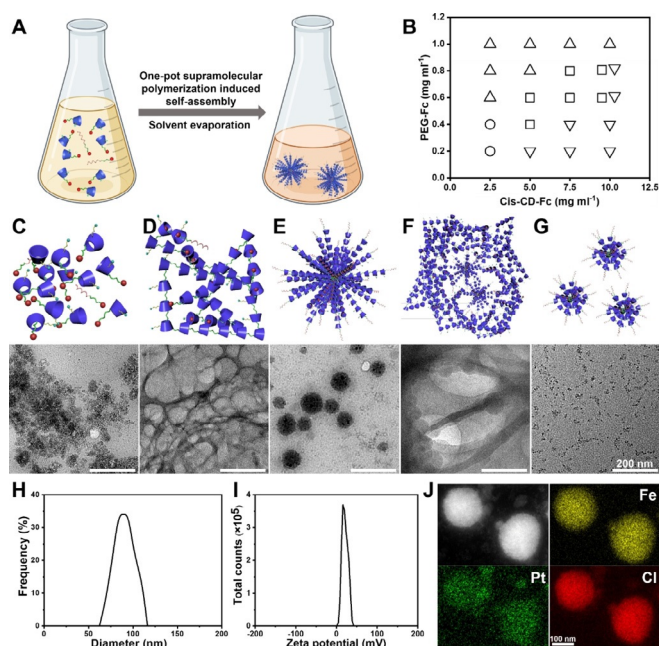


Figure 1. Synthesis and characterizations of PCSNs. (A) One-pot supramolecular polymerization-induced self-assembly of Cis-CD-Fc monomers. (B) The product diagram for the self-assembly of SPs with varying amounts of Cis-CD-Fc monomers and PEG-Fc. (○) irregular aggregates, (▽) microfibers, (□) nanoparticles, (□▽) mixture of nanoparticles and microfibers and (△) ultrasmall nanodots. (C–G) Representative TEM images of (C) irregular aggregates, (D) microfibers, (E) nanoparticles, (F) mixture of nanoparticles and microfibers and (G) ultrasmall nanodots assembled from SPs of various concentrations of Cis-CD-Fc monomers and PEG-Fc. (H) Hydrodynamic diameter, (I) zeta potential and (J) EDS element mapping of PCSNs.

SNs. Therefore, SPs of Cis-CD-Fc were employed to construct PCSNs for further investigations.

H₂O₂-Responsive Dissociation of PCSNs, Generation of ROS and Release of Platinum (IV) Prodrug

PCSNs were incubated with a H₂O₂ solution at an endogenous concentration (100 μM) to evaluate the H₂O₂-responsiveness of the nanoassemblies *in vitro*.^[20] The corresponding morphology and size changes of PCSNs were clearly observed by TEM and DLS analysis (Figure 2 A,B). PCSNs were rapidly dissociated within 0.5 h and completely disassembled after 2 h incubation in the H₂O₂ solution, owing to the weakened binding affinity between CD and Fc that was oxidized by H₂O₂ via a Fenton-like reaction. The dissociation of PCSNs was accompanied by the generation of hydroxyl radicals for potential CDT, which was evaluated by using methylene blue (MB) as an indicator (Figure 2C). In the presence of H₂O₂, both CD-Fc-based SNs (CSNs) and PCSNs led to a significant decrease in the absorbance of MB at 550–700 nm, while no apparent changes in the absorbance were observed for MB solutions cultured with H₂O₂ or SNs alone, suggesting the degradation of MB by the hydroxyl radicals generated via a Fenton-like reaction between H₂O₂ and SNs. The H₂O₂-induced dissociation of PCSNs was further verified by monitoring the release of platinum (IV) complex (Figure 2D). In the absence of H₂O₂, little release of platinum (IV) complex (< 9%) from PCSNs was detected for up to 24 h, indicating the great stability and limited premature leakage of the nanoparticles. In contrast, over 91% of platinum (IV) prodrug was released from PCSNs within 6 h incubation in a H₂O₂ solution (100 μM), demonstrating the H₂O₂-induced dissociation of PCSNs and subsequent release of platinum (IV) prodrug from the nanoassemblies. In addition to the H₂O₂-responsive release of platinum (IV) prodrug, ferrocene was also rapidly released from the supramolecular nanoassemblies in the presence of H₂O₂,

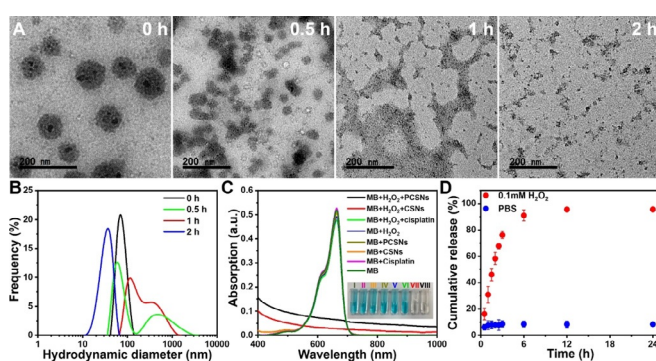


Figure 2. H₂O₂-responsive dissociation of PCSNs. (A) TEM images of PCSNs after incubation with H₂O₂ (100 μM) for various time durations and (B) the corresponding hydrodynamic diameters of PCSNs under H₂O₂ incubation. (C) UV/Vis spectra of MB solution after reaction with various formulations for 20 min. Inset photos indicated the color changes before and after the reaction. (D) *In vitro* release of platinum (IV) prodrug from PCSNs in the presence and absence of H₂O₂ (100 μM), respectively. Data are presented as means ± S.D. (*n* = 5).

suggesting the potential of PCSNs in selective tumor therapy (Figure S23).

In Vitro Cell Internalization, ROS Generation and Antitumor Efficacy

Fluorescent PCSNs were fabricated by conjugating Cy7 onto PEG-Fc for supramolecular polymerization-induced self-assembly to investigate the cellular internalization of Cy7-labelled PCSNs (Figure S24–S26). After incubation with Cy7-labelled PCSNs, the fluorescent intensity in 4T1 cells was gradually enhanced with increasing incubation time, indicating that the PCSNs could be delivered into tumor cells effectively over time (Figure S27 and S28). Subsequently, the generation of hydroxyl radicals in 4T1 cells induced by PCSNs was evaluated by using the intracellular ROS probe 2',7'-dichlorofluorescein diacetate (DCFH-DA), which could be oxidized by hydroxyl radicals into highly emissive DCF. According to the confocal observation, negligible fluorescence was found in 4T1 cells treated with PBS or cisplatin, indicating the relatively low ROS levels in these groups (Figure 3A). Only a slight enhancement in green fluorescence

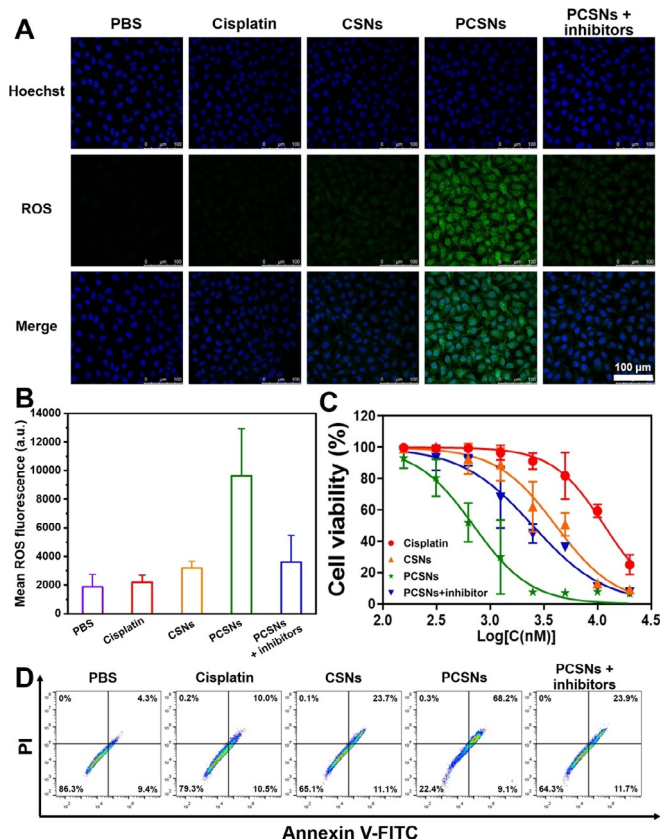


Figure 3. *In vitro* ROS generation and anticancer activity of PCSNs. (A) Confocal laser scanning microscopy images for ROS measurement of 4T1 cells after various treatment (Green fluorescence indicates the ROS level) and (B) the corresponding quantitative analysis of intracellular ROS level by flow cytometry. (C) Cell viability and (D) Annexin V-FITC/PI dual staining assays of 4T1 cells after incubation with various formulations for 24 h. Data are presented as means ± S.D. (*n* = 5).

was observed in cells incubated with CSNs or PCSNs plus sodium pyruvate as H_2O_2 scavengers, possibly owing to the deficient endogenous H_2O_2 to generate enough hydroxyl radicals via the Fenton-like reaction.^[21] In contrast, strong ROS fluorescence appeared in cells treated with PCSNs, attributed to the elevated intracellular H_2O_2 concentration induced by the released platinum (IV) prodrug. Similar results were also found via flow cytometry analysis, where PCSNs-treated cells demonstrated 3.0- and 2.7-fold enhancement in ROS fluorescence than the cells incubated with CSNs or PCSNs plus sodium pyruvate, respectively (Figure 3B and S29).

Encouraged by the efficient intracellular generation of hydroxyl radicals induced by PCSNs, we further evaluated the potential cytotoxicity of the nanoparticles via the MTT assay. Free cisplatin, CSNs and PCSNs plus sodium pyruvate were employed as control groups. As illustrated in Figure 3C, all groups exhibited a dose-dependent cytotoxicity on 4T1 cells. However, PCSNs exhibited the strongest cytotoxicity against 4T1 cells with the half maximal inhibitory concentration (IC_{50}) of 702.1 ± 107.6 nM (based on the molar amount of Pt in supramolecular monomers), which is 16.5- and 5.8-fold lower than that of cisplatin and CSNs under the identical Pt and Fe concentrations, respectively. This could be attributed to the self-amplified dissociation of PCSNs and thereafter the burst release of platinum (IV) prodrug as well as the elevated generation of ROS within tumor cells. Notably, the viability of 4T1 cells incubated with PCSNs plus sodium pyruvate was significantly enhanced when compared with cells treated with PCSNs, further confirming the synergistic chemo/chemodynamic effect of PCSNs via platinum drug-promoted H_2O_2 production. In addition, PCSNs exhibited identical cytotoxicity on 4T1 cells with various initial concentrations of H_2O_2 in the culture medium, while low toxicity was observed in cells cultured with H_2O_2 at all concentrations, indicating that PCSNs could effectively inhibit tumor cell growth on the basis of endogenous H_2O_2 (Figure S30). An Annexin V-FITC/propidium iodide (PI) dual-staining assay was performed to investigate the apoptosis and necrosis of 4T1 cells incubated with PCSNs (Figure 3D). Compared with cells treated with PBS, cisplatin, CSNs or PCSNs plus sodium pyruvate, much higher rate of apoptosis (77.3%) was detected for the 4T1 cells incubated with PCSNs, suggesting the remarkable cell growth inhibitory effect of PCSNs owing to the synergistic effect of self-amplified ROS generation and platinum (IV) complex release.

In Vivo Biodistribution and Antitumor Performance of PCSNs

To investigate the delivery, accumulation and excretion of the nanomedicine, Cy7-labelled PCSNs were intravenously injected into 4T1 tumor-bearing BALB/c mice and the mice were imaged via an in vivo imaging system (IVIS) at scheduled time points after intravenous injection to trace the distribution of the nanoassemblies (Figure 4A). The fluorescence signals at the tumor site showed a gradual increase after the injection of the nanoassemblies and reached maximum intensity at 6 h post-injection, suggesting the time-

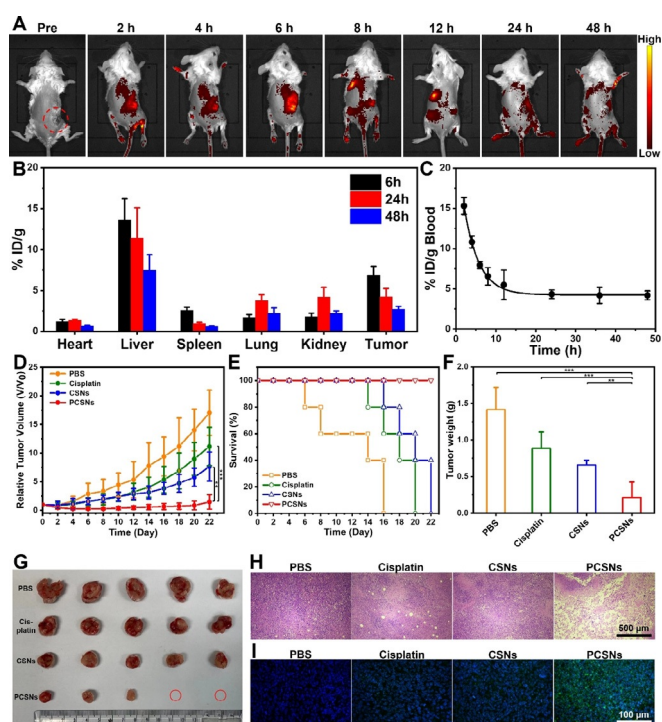


Figure 4. Biodistribution and anticancer efficacy of PCSNs in vivo. (A) In vivo fluorescence images of 4T1 tumor-bearing BALB/c mice at different time points after intravenous injection of Cy7-labelled PCSNs. (B) Biodistribution of platinum-based nanomedicine in the major organs and tumors at different time points post injection of Cy7-labelled PCSNs. (C) Blood clearance of PCSNs in 4T1 tumor-bearing mice. (D) The tumor volume evolution curves, (E) survival curves, (F) final tumor weight and (G) photographs of the dissected tumors by the end of treatment. (H) H&E and (I) TUNEL staining of tumor sections collected from mice intravenously injected with PBS, cisplatin, CSNs and PCSNs, respectively. Data are presented as means \pm S.D ($n=5$). (** $p < 0.001$, ** $p < 0.01$, * $p < 0.05$).

dependent accumulation of Cy7-labelled PCSNs in the tumor, likely due to the EPR effect. Notably, a significant increase in fluorescence was observed in the kidney at 8 h post-injection of the nanomedicines, indicating the potential excretion of dissociated nanoassemblies via renal clearance. In a separate study, the 4T1 tumor-bearing mice were sacrificed at different time points after injection of Cy7-labelled PCSNs and the tumors as well as major organs were harvested for quantitative ex vivo imaging and ICP-MS analysis of Pt content (Figure 4B and S31). The Pt content in the tumors increased to 6.85 ± 1.11 % ID g^{-1} at 6 h and then decreased gradually to 4.23 ± 1.02 % ID g^{-1} at 24 h post-injection. In contrast, the Pt content in the kidney increased from 1.81 ± 0.44 % ID g^{-1} at 6 h to 4.22 ± 1.16 % ID g^{-1} at 24 h post-injection of Cy7-labelled PCSNs, implying the renal clearance of the supramolecular nanoassemblies after their dissociation in the tumors. The systemic circulation and clearance of supramolecular nanoparticles was also investigated by monitoring the content of Pt over time in the blood and urine of the PCSNs-treated 4T1 tumor-bearing mice (Figure 4C and S32). The clearance of PCSNs in the blood followed a simple exponential decay curve, with a half-life of ≈ 6.4 h. In

contrast, the Pt content in the urine increased gradually within 12 h post-injection of PCSNs, further confirming that the nanoassemblies could be readily dissociated and excreted from the body via renal clearance to avoid the potential side effects.^[22]

Inspired by the excellent *in vitro* anticancer results and satisfactory tumor accumulation, we evaluated the *in vivo* antitumor performance of PCSNs on 4T1 tumor-bearing mice. When the tumor volume exceeded 100 mm³, the mice were randomly divided into four groups and intravenously injected with PBS, cisplatin, CSNs and PCSNs, respectively (equivalent Pt dose of 2 mg kg⁻¹, equivalent Fc dose of 2.5 mg kg⁻¹). The tumor sizes were closely monitored every two days in each group to identify the tumor growth inhibition effect (Figure S33). As shown in Figure 4D, the mice treated with PBS exhibited a rapid increase in the tumor volume. A modest delay in tumor growth was observed in the mice treated with cisplatin or CSNs, likely owing to moderate therapeutic effects of individual chemotherapy or CDT. In contrast, the mice treated with PCSNs displayed significantly suppressed tumor growth, suggesting the desirable synergistic therapeutic effect of self-augmented cascade ROS generation and platinum (IV) complex release. This was also verified by the prolonged survival time, reduced tumor weight and volume of PCSNs-treated mice at the end of treatment, when compared with all the other treatment groups (Figure 4E–G). In addition, the administration of PCSNs led to the highest level of apoptosis and necrosis in the tumor tissues in comparison with other groups, as revealed by the hematoxylin and eosin (H&E) staining and the terminal deoxynucleotidyl transferase dUTP nick end labeling (TUNEL) staining of the tumor tissue sections, convincingly confirming the excellent anticancer efficacy of PCSNs via self-amplified synergistic chemo/chemodynamic therapy (Figure 4H,I).

Systemic Toxicity Evaluation

The systemic toxicity of the formulations was first evaluated by monitoring the body weight changes of the mice during the therapeutic period (Figure 5A and S34). Compared with other groups, a rapid loss in body weight was observed for the mice treated with free cisplatin, indicating severe side effects induced by the nonspecific distribution of cisplatin. By incorporating platinum (IV) complex into the PCSNs, the toxicity was significantly reduced at the same dosage as revealed by the negligible body weight reduction of the PCSNs-treated mice. Additionally, no evident symptoms of toxic effects on eating, drinking, urination, grooming, physical/social activity and neurological status occurred in the mice administered with PCSNs, suggesting the low systemic toxicity of PCSNs during the treatment period.

To further evaluate the potential toxicity of PCSNs, blood was collected from the mice on Day 1 and Day 14 after intravenous administration with different formulations for blood biochemistry and hematology analysis (Figure 5B–P). An obvious increase in kidney function related markers (BUN, CREA and UA) and a significant reduction in white blood cells (WBC) and lymphocytes (LYM) was observed in

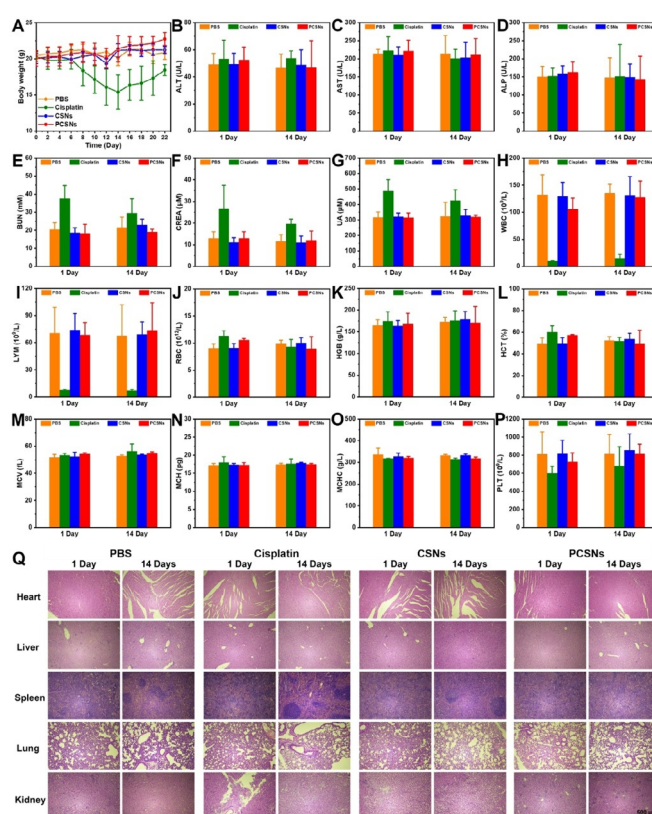


Figure 5. *In vivo* safety evaluation of intravenously administered PCSNs. (A) Body weight variation of 4T1 tumor-bearing BALB/c mice intravenously administered with PBS, cisplatin, CSNs and PCSNs, respectively. (B–D) Quantitative analysis of liver function biomarkers (ALT, AST and ALP) and (E–G) kidney function biomarkers (BUN, CREA and UA) in the blood of the mice after various treatments. (H–P) The levels of (H) white blood cells, (I) lymphocytes, (J) red blood cells, (K) hemoglobin, (L) hematocrit, (M) mean corpuscular volume, (N) mean corpuscular hemoglobin, (O) mean corpuscular hemoglobin concentration and (P) platelets in mice treated with PBS, cisplatin, CSNs and PCSNs, respectively. (Q) H&E staining of major organs from the mice after various treatments for 1 and 14 days. Data are presented as means \pm S.D. ($n = 5$). (*** $p < 0.001$, ** $p < 0.01$, * $p < 0.05$).

mice injected with cisplatin, indicating the severe nephrotoxicity and hematopoietic stem cell toxicity of free drugs.^[23] In contrast, no apparent changes in these parameters were found in mice treated with PBS, CSNs and PCSNs within the experimental period, indicating the significantly reduced toxicity of platinum (IV) complex-bearing PCSNs. In addition, all the liver function related markers (ALT, AST and ALP) and other hematological indicators including red blood cell count (RBC), hemoglobin (HGB), hematocrit (HCT), mean corpuscular volume (MCV), mean corpuscular hemoglobin (MCH), mean corpuscular hemoglobin concentration (MCHC) and platelet count (PLT) were in the normal range for the mice injected with PCSNs, indicating the desirable blood safety of the nanoassemblies.

H&E staining of major organs was employed to assess the potential *in vivo* toxicity of various formulations (Figure 5Q). It is worth noting that cisplatin-treated mice showed significant apoptosis and necrosis in the kidney tissues while no

observable tissue damage, inflammatory lesion or accumulation of inflammatory immune cells was found in the PCSNs-treated mice as compared with the control group, further confirming the reduced systemic toxicity of platinum drugs by PCSNs, likely owing to the tumor-specific dissociation and rapid renal clearance of the supramolecular nanoassemblies.

Conclusion

In summary, we have developed a H₂O₂-responsive nanomedicine via one-pot supramolecular polymerization-induced self-assembly of Cis-CD-Fc monomers with the Fenton catalyst Fc as the guest and CD as the host. The resultant PCSNs possessed high drug loading content and tunable ratio of platinum (IV) complex and Fc. In the presence of endogenous H₂O₂ overproduced in tumor tissues, the PCSNs could be dissociated rapidly to release hydroxyl radicals and platinum (IV) prodrug, which was reduced to chemotherapeutic cisplatin and promoted the generation of H₂O₂ in tumor tissues, thus leading to self-augmented anticancer performance through cascade ROS generation and drug release. Moreover, the PCSNs exhibited excellent biocompatibility and minimized side effects based on the evaluation of body weight, blood biochemistry, and various organs' histological analysis, likely owing to the tumor-specific release of platinum (IV) prodrug as well as the rapid renal clearance of the nanocarriers after their dissociation. Therefore, this supramolecular polymeric nanomedicine is anticipated to find clinical translation in combating tumors with high H₂O₂ levels via synergistic chemo/chemodynamic therapy and offer new insights on the design and development of supramolecular polymers for cancer theranostics.

Acknowledgements

This study was financially supported by National Natural Science Foundation of China (21871301 and 22071275), the Science and Technology Development Fund, Macau SAR (SKL-QRCM(UM)-2020-2022), the National University of Singapore Startup Fund (NUHSRO/2020/133/Startup/08) and the NUS School of Medicine Nanomedicine Translational Research Programme (NUHSRO/2021/034/TRP/09/Nano-medicine). K.Y. is supported by the UM Macao Postdoctoral Fellowship.

Conflict of Interest

The authors declare no conflict of interest.

Keywords: drug delivery · self-amplified dissociation · self-assembly · supramolecular polymerization · synergistic chemo/chemodynamic therapy

- [1] a) Z. Tang, Y. Liu, M. He, W. Bu, *Angew. Chem. Int. Ed.* **2019**, *58*, 946–956; *Angew. Chem.* **2019**, *131*, 958–968; b) L.-S. Lin, J.

- Song, L. Song, K. Ke, Y. Liu, Z. Zhou, Z. Shen, J. Li, Z. Yang, W. Tang, G. Niu, H.-H. Yang, X. Chen, *Angew. Chem. Int. Ed.* **2018**, *57*, 4902–4906; *Angew. Chem.* **2018**, *130*, 4996–5000; c) H. Lin, Y. Chen, J. Shi, *Chem. Soc. Rev.* **2018**, *47*, 1938–1958.
- [2] a) L. Zhang, S.-S. Wan, C.-X. Li, L. Xu, H. Cheng, X.-Z. Zhang, *Nano Lett.* **2018**, *18*, 7609–7618; b) L.-S. Lin, T. Huang, J. Song, X.-Y. Ou, Z. Wang, H. Deng, R. Tian, Y. Liu, J.-F. Wang, Y. Liu, G. Yu, Z. Zhou, S. Wang, G. Niu, H.-H. Yang, X. Chen, *J. Am. Chem. Soc.* **2019**, *141*, 9937–9945; c) C. Liu, D. Wang, S. Zhang, Y. Cheng, F. Yang, Y. Xing, T. Xu, H. Dong, X. Zhang, *ACS Nano* **2019**, *13*, 4267–4277; d) X. Wang, X. Zhong, Z. Liu, L. Cheng, *Nano Today* **2020**, *35*, 100946.
- [3] a) J. J. Wilson, S. J. Lippard, *Chem. Rev.* **2014**, *114*, 4470–4495; b) S. Ghosh, *Bioorg. Chem.* **2019**, *88*, 102925; c) X. Wang, X. Wang, Z. Guo, *Acc. Chem. Res.* **2015**, *48*, 2622–2631.
- [4] H.-J. Kim, J.-H. Lee, S.-J. Kim, G. S. Oh, H.-D. Moon, K.-B. Kwon, C. Park, B. H. Park, H.-K. Lee, S.-Y. Chung, R. Park, H.-S. So, *J. Neurosci.* **2010**, *30*, 3933–3946.
- [5] a) Y. Dai, Z. Yang, S. Cheng, Z. Wang, R. Zhang, G. Zhu, Z. Wang, B. C. Yung, R. Tian, O. Jacobson, C. Xu, Q. Ni, J. Song, X. Sun, G. Niu, X. Chen, *Adv. Mater.* **2018**, *30*, 1704877; b) P. A. Ma, H. Xiao, C. Yu, J. Liu, Z. Cheng, H. Song, X. Zhang, C. Li, J. Wang, Z. Gu, J. Lin, *Nano Lett.* **2017**, *17*, 928–937; c) Z. Ren, S. Sun, R. Sun, G. Cui, L. Hong, B. Rao, A. Li, Z. Yu, Q. Kan, Z. Mao, *Adv. Mater.* **2020**, *32*, 1906024.
- [6] Z. Yang, Y. Dai, C. Yin, Q. Fan, W. Zhang, J. Song, G. Yu, W. Tang, W. Fan, B. C. Yung, J. Li, X. Li, X. Li, Y. Tang, W. Huang, J. Song, X. Chen, *Adv. Mater.* **2018**, *30*, 1707509.
- [7] a) H. Su, Y. Cui, F. Wang, W. Zhang, C. Zhang, R. Wang, H. Cui, *Biomater. Sci.* **2021**, *9*, 463–470; b) Y. Huo, Z. He, C. Wang, L. Zhang, Q. Xuan, S. Wei, Y. Wang, D. Pan, B. Dong, R. Wei, N. Naik, Z. Guo, *Chem. Commun.* **2021**, *57*, 1413–1429; c) Q. Luo, Z. Dong, C. Hou, J. Liu, *Chem. Commun.* **2014**, *50*, 9997–10007; d) H. Wang, Y.-Q. Yan, Y. Yi, Z.-Y. Wei, H. Chen, J.-F. Xu, H. Wang, Y. Zhao, X. Zhang, *CCS Chem.* **2020**, *2*, 739–748.
- [8] a) X. Jin, L. Zhu, B. Xue, X. Zhu, D. Yan, *Natl. Sci. Rev.* **2019**, *6*, 1128–1137; b) T. Kakuta, T.-a. Yamagishi, T. Ogoshi, *Acc. Chem. Res.* **2018**, *51*, 1656–1666; c) P. Wang, J. Ma, D. Xia, *Org. Chem. Front.* **2018**, *5*, 1297–1302.
- [9] a) X.-M. Chen, Y. Chen, Q. Yu, B.-H. Gu, Y. Liu, *Angew. Chem. Int. Ed.* **2018**, *57*, 12519–12523; *Angew. Chem.* **2018**, *130*, 12699–12703; b) G. Yu, X. Zhao, J. Zhou, Z. Mao, X. Huang, Z. Wang, B. Hua, Y. Liu, F. Zhang, Z. He, O. Jacobson, C. Gao, W. Wang, C. Yu, X. Zhu, F. Huang, X. Chen, *J. Am. Chem. Soc.* **2018**, *140*, 8005–8019.
- [10] a) J. Tan, H. Li, X. Hu, R. Abdullah, S. Xie, L. Zhang, M. Zhao, Q. Luo, Y. Li, Z. Sun, Q. Yuan, W. Tan, *Chem* **2019**, *5*, 1775–1792; b) Y. Wang, W. Yin, W. Ke, W. Chen, C. He, Z. Ge, *Biomacromolecules* **2018**, *19*, 1990–1998; c) F. M. Menger, M. J. Sherrod, *J. Am. Chem. Soc.* **1988**, *110*, 8606–8611; d) H. J. Thiem, M. Brandl, R. Breslow, *J. Am. Chem. Soc.* **1988**, *110*, 8612–8616.
- [11] a) C. Fang, Z. Deng, G. Cao, Q. Chu, Y. Wu, X. Li, X. Peng, G. Han, *Adv. Funct. Mater.* **2020**, *30*, 1910085; b) Z. Deng, C. Fang, X. Ma, X. Li, Y.-J. Zeng, X. Peng, *ACS Appl. Mater. Interfaces* **2020**, *12*, 20321–20330.
- [12] a) X. Xu, Z. Zeng, J. Chen, B. Huang, Z. Guan, Y. Huang, Z. Huang, C. Zhao, *Chem. Eng. J.* **2020**, *390*, 124628; b) S. Yi, J. Zheng, P. Lv, D. Zhang, X. Zheng, Y. Zhang, R. Liao, *Bioconjugate Chem.* **2018**, *29*, 2884–2891.
- [13] a) G.-Y. Liou, P. Storz, *Free Radical Res.* **2010**, *44*, 479–496; b) J. Liu, Y. Li, S. Chen, Y. Lin, H. Lai, B. Chen, T. Chen, *Front. Chem.* **2020**, *8*, 838; c) T. P. Szatrowski, C. F. Nathan, *Cancer Res.* **1991**, *51*, 794; d) Y. Yu, J. Peng, M. Pan, Y. Ming, Y. Li, L. Yuan, Q. Liu, R. Han, Y. Hao, Y. Yang, D. Hu, H. Li, Z. Qian, *Small Methods* **2021**, *5*, 2001212.

- [14] a) Y. Sun, F. Guo, T. Zuo, J. Hua, G. Diao, *Nat. Commun.* **2016**, *7*, 12042; b) W. S. Jeon, K. Moon, S. H. Park, H. Chun, Y. H. Ko, J. Y. Lee, E. S. Lee, S. Samal, N. Selvapalam, M. V. Rekharsky, V. Sindelar, D. Sobransingh, Y. Inoue, A. E. Kaifer, K. Kim, *J. Am. Chem. Soc.* **2005**, *127*, 12984–12989.
- [15] a) M. Miyauchi, Y. Takashima, H. Yamaguchi, A. Harada, *J. Am. Chem. Soc.* **2005**, *127*, 2984–2989; b) Y.-K. Tian, Y.-G. Shi, Z.-S. Yang, F. Wang, *Angew. Chem. Int. Ed.* **2014**, *53*, 6090–6094; *Angew. Chem.* **2014**, *126*, 6204–6208.
- [16] a) K. Knop, R. Hoogenboom, D. Fischer, U. S. Schubert, *Angew. Chem. Int. Ed.* **2010**, *49*, 6288–6308; *Angew. Chem.* **2010**, *122*, 6430–6452; b) F. M. Veronese, G. Pasut, *Drug Discovery Today* **2005**, *10*, 1451–1458; c) H. Otsuka, Y. Nagasaki, K. Kataoka, *Adv. Drug Delivery Rev.* **2003**, *55*, 403–419; d) J. S. Suk, Q. Xu, N. Kim, J. Hanes, L. M. Ensign, *Adv. Drug Delivery Rev.* **2016**, *99*, 28–51.
- [17] a) H. Maeda, J. Wu, T. Sawa, Y. Matsumura, K. Hori, *J. Controlled Release* **2000**, *65*, 271–284; b) J. Fang, H. Nakamura, H. Maeda, *Adv. Drug Delivery Rev.* **2011**, *63*, 136–151; c) A. Albanese, P. S. Tang, W. C. W. Chan, *Annu. Rev. Biomed. Eng.* **2012**, *14*, 1–16.
- [18] T. Mosmann, *J. Immunol. Methods* **1983**, *65*, 55–63.
- [19] a) T.-C. Chou, P. Talalay, *Adv. Enzyme Regul.* **1984**, *22*, 27–55; b) T.-C. Chou, *Pharmacol. Rev.* **2006**, *58*, 621.
- [20] B. Halliwell, M. V. Clement, L. H. Long, *FEBS Lett.* **2000**, *486*, 10–13.
- [21] a) S. Desagher, J. Glowinski, J. Prémont, *J. Neurosci.* **1997**, *17*, 9060; b) N. Kaushik, N. Uddin, G. B. Sim, Y. J. Hong, K. Y. Baik, C. H. Kim, S. J. Lee, N. K. Kaushik, E. H. Choi, *Sci. Rep.* **2015**, *5*, 8587; c) S. Wang, G. Yu, Z. Wang, O. Jacobson, L.-S. Lin, W. Yang, H. Deng, Z. He, Y. Liu, Z.-Y. Chen, X. Chen, *Angew. Chem. Int. Ed.* **2019**, *58*, 14758–14763; *Angew. Chem.* **2019**, *131*, 14900–14905; d) Y. Sang, F. Cao, W. Li, L. Zhang, Y. You, Q. Deng, K. Dong, J. Ren, X. Qu, *J. Am. Chem. Soc.* **2020**, *142*, 5177–5183.
- [22] M. Longmire, P. L. Choyke, H. Kobayashi, *Nanomedicine* **2008**, *3*, 703–717.
- [23] a) N. Pabla, Z. Dong, *Kidney Int.* **2008**, *73*, 994–1007; b) X. Yao, K. Panichpisal, N. Kurtzman, K. Nugent, *Am. J. Med. Sci.* **2007**, *334*, 115–124; c) B. Das, R. Antoon, R. Tsuchida, S. Lotfi, O. Morozova, W. Farhat, D. Malkin, G. Koren, H. Yeger, S. Baruchel, *Neoplasia* **2008**, *10*, 1105-IN1104.

Manuscript received: March 15, 2021

Revised manuscript received: May 5, 2021

Accepted manuscript online: May 26, 2021

Version of record online: June 27, 2021